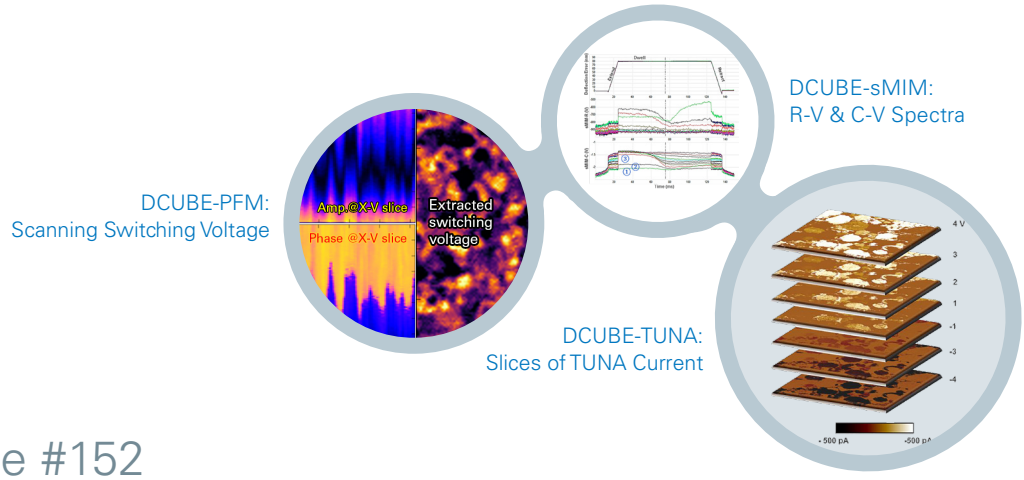

Application Note #152

Performing Hyperspectral Mapping with AFM DataCube Nanoelectrical Modes

AFM-based nanoelectrical modes have found applications in fields ranging from semiconductors to piezoelectric materials, energy research, and biology. Modes are available to characterize the local conductivity, resistivity, charge, carrier concentration, carrier-type, or piezoelectric properties with nanometer-scale spatial resolution, and usually require a direct contact between the AFM tip and sample. The data produced have traditionally been in the form of a two-dimensional (2D) map, generated in contact mode, with a single electrical data point per XY location. At few, carefully selected locations in this map, electrical ramps or spectra are generated to get a deeper insight in the local electrical properties. This application note introduces a new approach to nanoelectrical imaging that goes beyond a 2D map, creating an entire electrical data cube and correlated nanomechanical data cube while operating at normal imaging speeds. This approach has the added benefit that it avoids contact mode imaging, thus extending electrical measurements to soft and fragile samples and improving measurement consistency through increased tip lifetime. Moreover, this is a general approach that is applicable to most nanoelectrical modes and applications. The more complete data set contains new information and enables functional imaging on complex samples as shown in examples of barrier height mapping in heterogeneous metal oxides, semiconductor carrier profiling, piezoelectric domain switching dynamics, and Li ion cathode characterization.

Moving Beyond Property Mapping

Atomic force microscopy is generally used to generate high-resolution (<1-5 nm) topographic images by raster scanning a sharp tip on the sample surface with feedback-controlled tip-sample force interactions. Bruker has pioneered AFM technology to simultaneously capture and extract mechanical properties from the tip-sample interactions. For example, PeakForce Quantitative Nanomechanics (PeakForce QNM®)[1-4] and FASTForce Volume™ (FFV)[5] modes provide an entire force curve for every pixel of the image, and the contact resonance mode[5] provides a resonance spectrum for every pixel of the image. From these spectra, mechanical properties such as adhesion, stiffness, modulus, deformation, tan-delta, and loss and storage modulus can be extracted and visualized in two-dimensional (2D) maps. For electrical characterization, a range of application modules is available,[6-9] and even electrical measurements in liquid are possible with the recent introduction of insulated AFM nanoelectrode probes for scanning electrochemical microscopy (SECM) and nanoelectrical characterization.[10-14] Having all of these capabilities contained within a single instrument provides researchers greater efficiency and experiment reach in both routine industrial applications and for highly multidisciplinary research in piezoelectricity, semiconductor devices, polymeric systems, energy research, and biological characterization.

AFM Nanoelectrical Modes

Conventional AFM nanoelectrical modes are generally operated with a fixed set of operating conditions (DC bias, AC bias, frequency, etc.) and a single electrical measurement is performed for every XY location, yielding a 2D electrical map. This is also true in PeakForce Tunneling AFM (PeakForce TUNA™)[6] and related PeakForce Tapping-based electrical modes,[7-9] which overcome the limitations of contact mode. Aside from 2D maps, AFM-based electrical characterization has long included point spectroscopy, whereby one of the operating conditions is swept as the tip is kept stationary, for example in the acquisition of current-voltage (I-V) curves at a single or a few selected individual positions. Point spectra can also be performed in arrays, but until now, this has remained rather time-consuming and has only allowed limited spatial sampling. Published application examples include capacitance-voltage (C-V) spectra applied for studying pn-junction delineation in Si devices,[15] and I-V spectra for investigating humidity effects on nanoscale electrochemistry in solid silver ion conductors.[16]

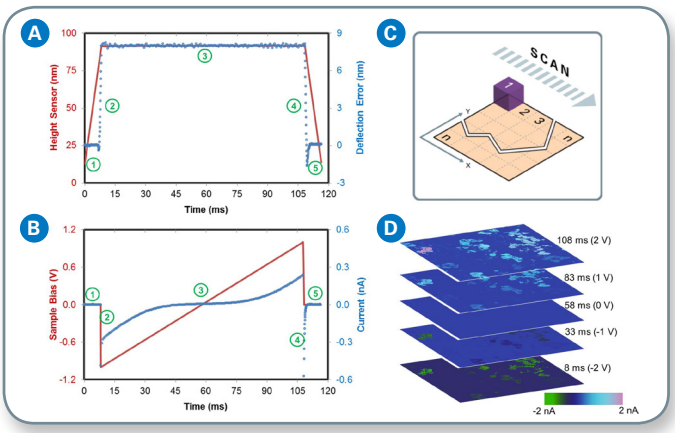

Figure 1. DCUBE modes operating on FFV approach: (a) height sensor (red) and deflection error (blue open circle) plots with segments showing extend (1–2), dwell (3), and retract (4–5) cycles; (b) pattern of sample bias (red) and corresponding TUNA current (blue); (c) illustration of scan pattern during acquisition of DCUBE-mode data; and (d) five TUNA current slices from the DCUBE-TUNA results.

DataCube Modes

Bruker's DataCube modes combine imaging and point spectroscopy, producing an integrated 3D data set. This multidimensional data cube measures the dependence of a specific electrical parameter in each XY position as a function of one of the (electrical) operating conditions.[17] The subjective approach of guessing locations of interest (for single-point spectroscopy) is replaced by a big data approach, resulting in higher dimensional data that can be sliced along any axis or plane, and which is conducive to principal component analysis and machine learning approaches to data reduction. The high dimensional electrical data sets allow one to extract high-resolution maps of electrical properties previously not acquired using AFM. Examples include images of Schottky barrier height, flat-band voltages, piezoelectric switching voltages, etc.

Rather than employing contact mode, the tip is moved from pixel to pixel in a FFV method.[5] An electrical spectrum is acquired during a hold segment inserted into each force curve in each pixel. The force curve at every pixel embedded in the FFV map constitutes a set of nanomechanical data cubes, which are spatially correlated with the electrical data cubes. Since the FFV map avoids lateral forces, tip lifetime is drastically improved and the electrical measurements are extended to polymers, nanoparticles, and other fragile samples that are impossible to study in contact mode. In this application note, the data cube principle is illustrated for tunneling AFM (TUNA), piezoforce microscopy (PFM), scanning capacitance microscopy (SCM), scanning spreading resistance microscopy (SSRM), and scanning microwave impedance microscopy (sMIM), but it can also be expanded to other electrical modes in both air and liquids.

Experimental Principle and Data Acquisition

Bruker's DataCube (DCUBE) modes are the result of seamless integration of existing high-performance nanoelectrical modes with the FFV technique. In the FFV mode, the tip is held in a fixed XY position, while a force distance cycle with "dwell" segment is executed in the Z direction. This is illustrated by the height sensor plot and corresponding force curve shown in Figure 1a. Force ramp rates up to 300 Hz are possible using Bruker's proprietary low-force trigger capability. Combined with sub-100 ms dwell times for the hold segment, good throughput is obtained and one can maintain regular imaging speeds also when acquiring dense arrays. In Figure 1a, the ramp rate for the "extend" and "retract" segments is 60 Hz at a normal force (or deflection) trigger level of 15 nN and with a Z movement of 80 nm. This results in a ramp speed of 9.6 µm/s.

During the "dwell" segment (here 100 ms), the sample bias is swept from -2 V to +2 V, corresponding to a ramp rate of 40 V/s, as shown in Figure 1b. The number of data points for the non-dwell and dwell segments can be set independently, allowing for high spectral resolution. In this example, 256 and 190 data points result in resolutions of 0.625 nm in Z and 21 mV in sample voltage, respectively. Higher density can be obtained by further increasing the amount of data points. The four spectra (height, deflection error, sample bias, and TUNA current) are captured simultaneously. After acquisition of the spectra in one pixel, the tip moves to the next pixel using the FFV raster scanning method (Figure 1c), avoiding the shear force common to contact mode–based scanning. Figure 1d shows five typical current slices extracted from a data cube acquired using this principle on a γ-Fe_2O_3 sample. Each current slice image consists of 256x256 pixels for a sample

area of 3x3 μm². The 190 spectral data points from the dwell segment provide 190 of these current slice images. At the same time, the "extend" / "retract" segments of the deflection plot construct a complete force-distance curve and allow one to extract quantitative nanomechanical images for modulus, adhesion, deformation, and stiffness.

In DCUBE modes, the conditions for force curve cycle and the electrical dwell period are controlled separately. This allows users to independently fine tune the measurement of force-distance spectra and electrical spectra. The duration of the hold segment for good quality signals depends on the nanoelectrical mode in use. More specifically, it depends on the applied AC frequency and/or the bandwidth of the sensor. As sensors normally have a bandwidth in the kHz range (for example; the PeakForce TUNA application module has a typical bandwidth of 15 kHz), acquisition times for capturing the whole electrical spectral down to ms level are possible. It is worthwhile to note that when increasing the electrical ramp speed, the signal/noise ratio will be compromised. For example, Figure 2 shows a series of capacitance-voltage (C-V) spectra of a p-type semiconductor captured by DCUBE-sMIM. These are raw data without averaging. The dwell time and the sample bias ramp rate for each spectrum are indicated on the figure. As shown by these results, a dwell time of 50 ms or a ramp rate of 80 V/s is sufficient to capture all the spectral features of this sample. Considering both force and electrical spectra, the time per pixel is typically in the range of 20-200 ms. For a 256x256 pixel map, this corresponds to an acquisition time of 22-220 min. Albeit, with this relatively long spectroscopic mapping duration, one can capture more than 1000 data points for each electrical spectrum, resulting in more than 1000 dynamic sequence or slice images at a capture rate of 1.3-13 s/image.

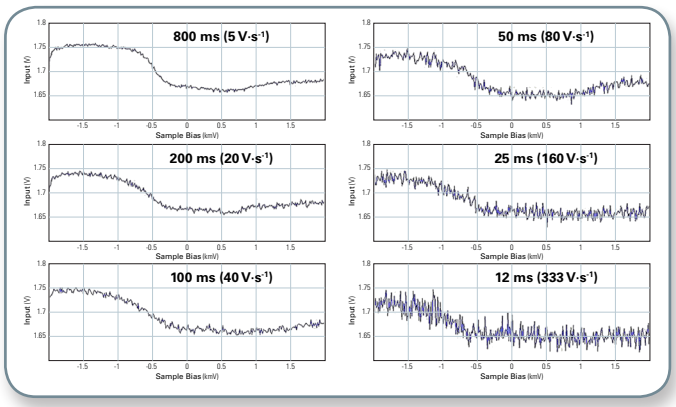

Figure 2. A series of C-V spectra of a p-type semiconductor captured by DCUBE-sMIM. These are raw data without averaging. The dwell time and the sample bias ramp rate for each spectrum are indicated.

As an alternative to ramping the DC sample bias during the dwell period, the user can also select to ramp any other parameter relevant to the electrical mode selected (e.g., the AC voltage, amplitude or frequency). In this way, one can collect a wide variety of electrical spectra, including I-V, C-V, dC/dV-V, R-V, dR/dV-V, PFM-amplitude-V, and

	Mechanical	Electrical				
	Force Volume	DCUBE-TUNA	DCUBE-SSRM	DCUBE-SCM	DCUBE-sMIM	DCUBE-PFM
Ramp Parameter	Distance	V_{DC}	V_{DC}	V_{DC} V_{AC} f_{AC} Phase	V_{DC} V_{AC} f_{AC} Phase	V_{DC} V_{AC} f_{AC} Phase
Output Channel	Force Stiffness Adhesion Modulus	Current	log(Resistance)	dC/dV Amplitude dC/dV Phase	dC/dV Amplitude dC/dV Phase sMIM-C sMIM-R	PFM Amplitude PFM Phase
Example Spectra	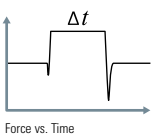 Force vs. Time	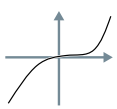 Current vs. V_{DC}	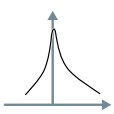 Log (resistance) vs. V_{DC}	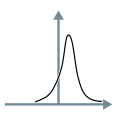 dC/dV vs. V_{DC}	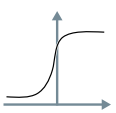 Capacitance vs. V_{DC}	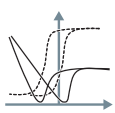 PFM vs. V_{DC}
				 dC/dV vs. V_{AC}	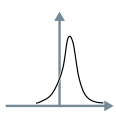 dC/dV vs. V_{DC}	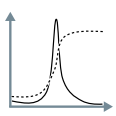 PFM vs. Frequency

Table 1. Summary of DCUBE modes and electrical characterizations with FFV.

PFM-amplitude-frequency spectra. Table 1 summarizes the available electrical DCUBE modes.

The electrical conditions can also be held constant during the dwell period, which can be short (milleseconds) or long (tens of seconds). In this way, the electrical signal can be averaged over a user-defined period, resulting in improved signal/noise ratios as compared to the equivalent contact or PeakForce electrical mode. During the dwell period, the electrical parameter is measured as a function of time, opening up the possibility to study time-dependent phenomena. Examples include mapping of time-dependent conductivity or photoconductivity after an external stimulus, such as a light pulse or electrical pulse; observing time-dependent dielectric breakdown in dielectrics; investigating charging or discharging effects after applying a voltage pulse; etc.

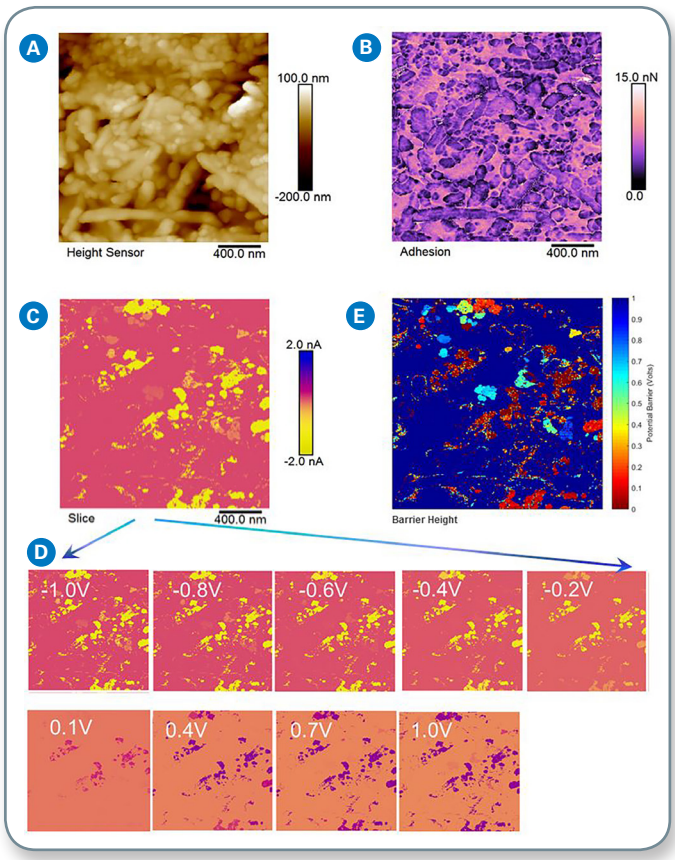

Figure 3. Processing, analysis, and visualization of DCUBE data. Slices of the spectroscopic maps can be extracted for regular processing of AFM images in NanoScope Analysis software: (a) surface topography; (b) quantitative nanomechanical properties—adhesion map; (c) a slice map from TUNA current—sample bias (I-V) spectra at -1 V (cover image of a movie created from 130 slices available on the Bruker website); (d) slices of TUNA current maps at selected voltages; and (e) scanning barrier height images created by analyzing all I-V spectra. The color bar displays from ohmic (zero) to insulating (one). NanoScope Analysis software goes with a MATLAB toolbox that allows one to extract the whole cube of data for further analysis in MATLAB. Image (e) was created by MATLAB.

Data Analysis

DCUBE modes provide simultaneous capture of nanometer-scale electrical and mechanical characteristics in high-density data cubes. For materials scientists and engineers, this breaks long-standing efficiency and characterization barriers. Processing such information-rich, big data results stimulates and encourages creative data mining. Bruker's standard NanoScope® analysis offline software provides a suite of data tools for basic processing and visualization, such as the extraction of individual slices and spectra. Figures 3 and 4 illustrate some of the core functions for handling DCUBE data (here, applied to DCUBE-TUNA data acquired on a γ-Fe_2O_3 sample).

First, slices of the spectroscopic maps can be extracted for further processing, as one would do with regular AFM images. This allows surface topography and quantitative nanomechanical maps to be extracted, as shown in Figure 3a and 3b. Figure 3c shows a current slice at a fixed sample bias of -1 V, while Figure 3d shows more current slices at nine selected voltages. Figure 4a shows a current slice at +2 V collected in a different area on the γ-Fe_2O_3 sample.

Second, one can select, display and export any of the spectra through single or multiple point selection in the surface topography, nanomechanical, or nanoelectrical images. One can also display and overlay all spectra from a selected region. Such a dense collection of spectra can also be visualized through statistical methods with the built-in density plots. An example is shown in Figure 4c created from 1890 spectra in the dashed-yellow-square region in Figure 4a. The darkness in this plot corresponds to the population density of the spectrum in this region of interest. In this particular example, the three visible curves in Figure 4c indicate three distinct electrical domain behaviors: insulating, low barrier, and high barrier.

Third, the NanoScope Analysis software also provides electrical contour plots along a user-defined line. Figure 4d shows the TUNA current changes over sample bias across the dashed-yellow line in Figure 4a. This is a 2D slice of the data cube at a fixed Y position, as indicated by the coordinates on the image. Each vertical line contains spectral information rendered by the false color of TUNA current. The (dark) blue-to-yellow stripes indicate the location along the line in Figure 4a where TUNA current changes with sample bias. The white plot on Figure 4d is the corresponding surface profile along the dashed-yellow line in Figure 4a, with a range of 150 nm in height. This shows that the nanoelectrical properties have no clear correlation with the surface topography and are only randomly varied among different particles.

Further in-depth analysis and data handling can also be performed using dedicated external analysis packages, such as MATLAB- or Python-based tools. For this purpose,

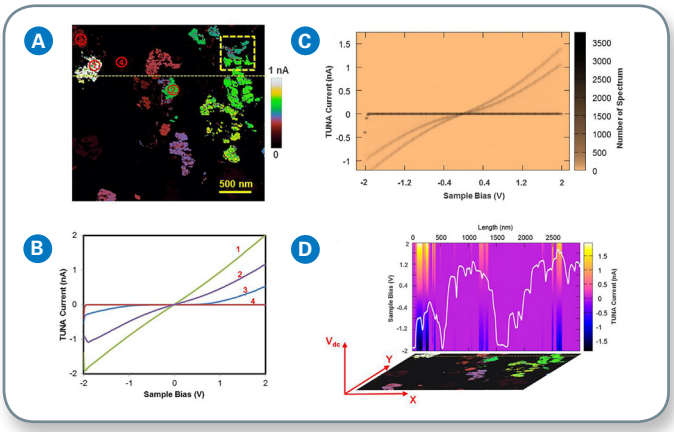

Figure 4. Processing, analysis, and visualization of nanoelectrical data from DCUBE-TUNA mode with NanoScope Analysis software: (a) current slice at +1 V; (b) point-selected I-V spectra as numbered in (a); (c) density plots based on 1890 I-V spectra from the dashed-yellow-square region in (a); and (d) TUNA current changes over sample bias across the dashed-yellow line in (a) where the white plot on the image is the corresponding surface profile with a range of 150 nm in height. This is a two-dimensional slice of the data cube at a fixed Y position as indicated by the coordinates on the image.

a toolbox is provided that allows one to directly import the DCUBE raw data files, and extract the channels of interest. These raw data files can be converted and also fed to other programming languages, such as Python. For example, one can create movies to show the electrodynamic of the materials. The TUNA current map in Figure 3c is the cover image of a movie created from 256 slices extracted from the data cube.[18] The sample bias ramping for this measurement is from -1 V to +1 V.

In a second example, MATLAB was used to perform a batch analysis of all I-V spectra in this data cube: Fitting the I-V spectra with a thermionic emission model allowed us to extract the barrier height of the metal tip / γ-Fe_2O_3 semiconductor Shockley junction. The resulting barrier height map is shown in Figure 3e and shows heterogeneity among different γ-Fe_2O_3 nanoparticles. The color bar represents from ohmic (zero) to insulating (one). This confirms previous studies by PeakForce TUNA and sMIM showing distinct electrical properties at the particle level.[8] This is a typical example of how the vast amount of data combined with in-depth analysis allows one to extract new, quantitative, nanoelectrical information previously unattainable by conventional AFM modes.

Case Study: DataCube Tunneling AFM (DCUBE-TUNA) on Li-Ion Battery Cathodes

Battery failure is a result of complex interrelated phenomena. It depends on battery chemistry, design, environment, and actual operation conditions.[20] Therefore, understanding, improving, and controlling the lifetime and performance of a battery requires studies at the component level. AFM has proven to be a powerful instrument for battery component studies.[21] However, the presence of materials with distinct mechanical properties, from soft (polymer additive), loose (conductive additive), to hard (Li metal oxide), porous (separator) surfaces, and high variation in surface topography, can pose challenges for contact-based scanning modes due to the nature of high normal imaging force and shear force. Tapping mode is superior to contact mode surface mapping in this regard. However, a majority of nanoelectrical characterization is based on solid tip-sample contact. Recently, PeakForce Tapping modes have proved useful for imaging challenging samples like battery materials,[22-26] in particular for in situ studies of the fragile solid electrolyte interphase layer on both anodes[27-29] and cathodes.[30,31] DCUBE modes further

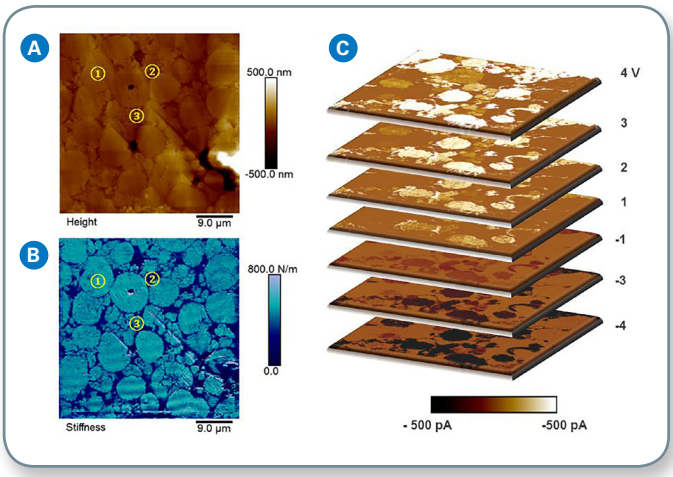

Figure 5. DCUBE-TUNA study of a battery cathode consisting of Li metal oxide (1), polymer binder (2), and conductive carbon nanoparticles (3): (a) surface topography; (b) quantitative surface stiffness differentiating different domains; and (c) a collection of TUNA current slices from the spectroscopic mapping at selected sample voltages. The scanning area is 45x45 µm^2.

expand the capabilities of PeakForce Tapping modes by enabling the acquisition of multidimensional data cubes through simultaneous capture of nanometer-scale electrical and mechanical characteristics in high-density data cubes.

The cathode investigated in this example consists of Li metal oxide, polymer binder, and conductive carbon nanoparticles. First, we scanned a large area of 45x45 µm^2, which can be challenging for other AFM nanoelectrical methods on this type of composite sample. Figure 5a shows a high-quality image of surface topography. The variation in height is over 1 µm, which is typical for a Li-ion battery cathode. Representative domains of Li metal oxide (1), polymer binder (2), and carbon black (3) are indicated on the images. These domains are better identified by Figure 5b, a quantitative map of surface stiffness, as Li metal oxide is of the hardest materials, and it shows the highest stiffness, whereas the polymer binder is the softest with the lowest stiffness. Figure 5c is a collection of slices from the spectroscopic mapping, showing the TUNA current image at selected sample bias, as indicated to the right. These TUNA current maps clearly show

distinct conductivities over different material domains, as well as conductivity heterogeneity over different Li metal oxide grains.

Figure 6 shows more details about this sample with a scan size of 15x15 μm², where the different material domains and the heterogeneity over different Li metal oxide grains are further presented. Figure 6a is the surface topography showing a few large Li metal oxide grains, e.g., regions #1–3. The inter-grain filling materials are difficult to identify on this morphology map. This is partially addressed by the stiffness and modulus maps in Figure 6b and 6c,

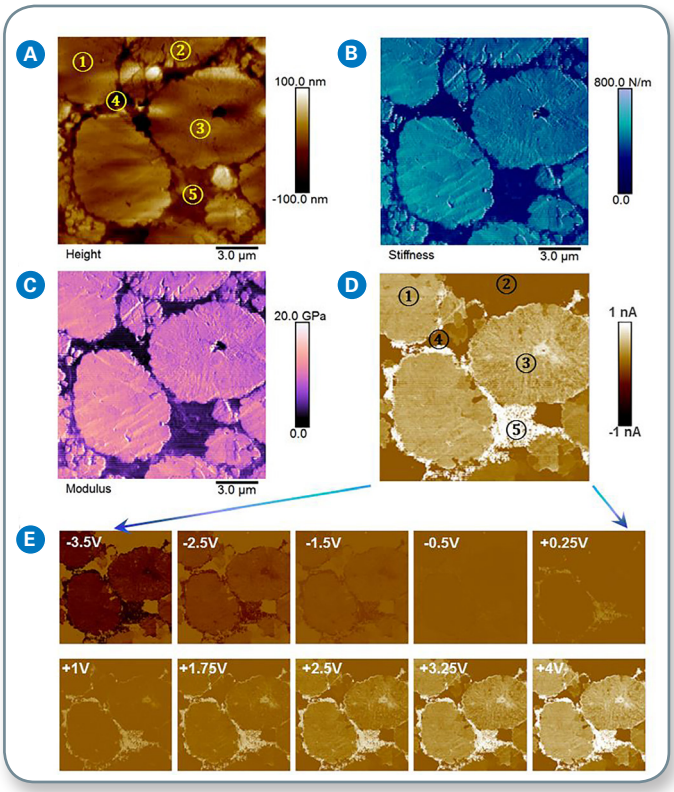

Figure 6. DCUBE-TUNA study of a battery cathode consisting of Li metal oxide (1)-(3), polymer binder (4), and conductive carbon nanoparticles (5): (a) surface topography; (b) quantitative surface stiffness differentiating different domains; (c) quantitative modulus map; and (d)-(e) TUNA current slices from the spectroscopic mapping at selected sample voltages. The scanning area is 15x15 μm².

where Li metal oxide shows high stiffness and modulus, respectively. This differentiation is confirmed by the TUNA current map in Figure 6d, a slice of spectroscopic mapping at a sample bias of +4 V. Carbon black rich regions (region #5) show high conductivity, while polymer binder regions are insulating (region #4). For the Li metal oxide domains, it is interesting that grain #2 only shows background current, which is totally different from other grains. This could be due to the lack of conduction channel connected by carbon black additives or by the intrinsic nature of the grain itself. Such a region needs to be avoided in practical design as it only serves as a redundant weight and volume burden to the battery, lowering the specific energy or volumetric energy density. In addition, the Li metal oxide also shows inner-grain heterogeneity, as indicated by grain #3 on Figure 6d. Figure 6e is a collection of slices from the spectroscopic mapping showing TUNA current images at selected sample biases as indicated. This series of images further confirms the electrical properties. More importantly, it shows the dynamic changes with applied sample biases from -4 V to +4 V. The current-voltage behaviors of the Li metal oxide grains deviate from linear Ohmic response. For example, the cathode is relatively silent to sample bias from -0.5 V to +0.25 V.

Figure 7 shows the DCUBE-TUNA results of a single Li metal oxide grain on this cathode. Surface topography in Figure 7a shows that this grain is an aggregate of sub-micron nanoparticles that have similar mechanical properties, as shown in the stiffness (Figure 7b) and modulus (Figure 7c). The TUNA current slices in Figure 8d and 8e extracted from the DCUBE-TUNA spectra at sample biases of +4 V and -4 V show conductivity variations amongst these particles. This confirms the inner-grain electrical heterogeneity shown in Figure 6d. Figure 7f plots all current-time spectra from the area indicated by the white square in Figure 7e. During this 125 ms dwell period,

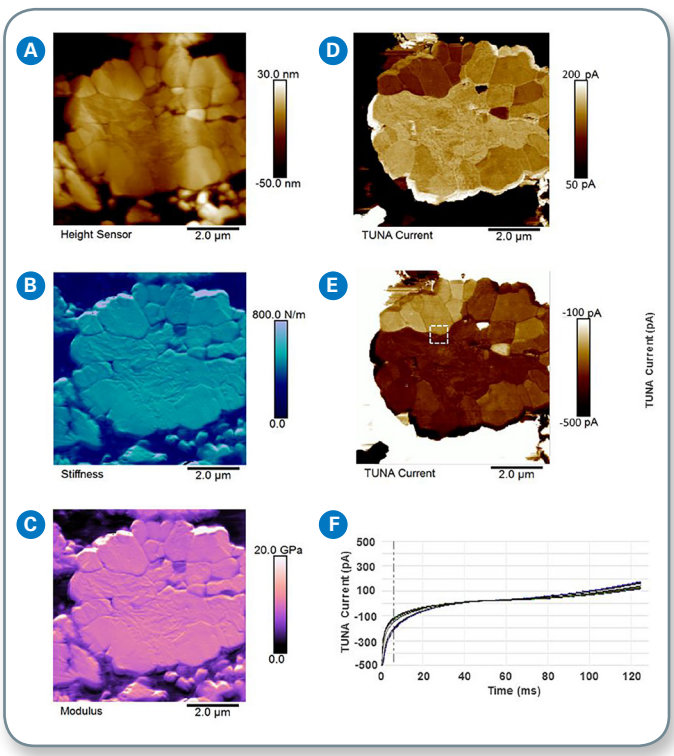

Figure 7. DCUBE-TUNA studies of a Li metal oxide grain on a battery cathode consisting of Li metal oxide, polymer binder, and conductive carbon nanoparticles: (a) surface topography; (b) map of quantitative surface stiffness differentiating different domains; (c) quantitative modulus map; (d)-(e) two slices from spectroscopic mapping showing TUNA current image at a sample bias of +4 V and -4 V, respectively; and (f) all current-time spectra from the area indicated by the white square in (e). During this 125 ms dwell period, the sample bias sweeps linearly from -4 V to +4 V, or at a rate of 64 V·s⁻¹.

the sample bias sweeps linearly from -4 V to +4 V, or at a rate of 64 V/s. The square area is across two nanoparticles with different conductivities, as shown in Figure 7e. Within each particle, the conductivity is relatively homogeneous. This results in two distinct groups of spectra, as shown in Figure 7e.

This DCUBE-TUNA example nicely demonstrates the importance of dynamic, multidimensional information for clearly differentiating and analyzing the performance of a complex system constructed from functional materials with distinct physical properties.

Case Study: DataCube Scanning Capacitance Microscopy (DCUBE-SCM) of Semiconductor Devices

SCM provides a method for direct measurement of activated carrier concentration with nanometer-scale accuracy in two dimensions. In SCM, the variation in carrier concentration inside semiconductor structures can be imaged through measurement of the dC/dV signal of the metal-oxide-semiconductor (MOS) capacitor formed by the probe and the semiconductor sample. In this mode, the probe is scanned in contact mode, and topography and electrical data are acquired simultaneously, enabling the direct correlation of a sample location with its electrical properties. Applications of SCM include failure analysis of semiconductor devices and two-dimensional carrier profiling of cross-sectioned semiconductor devices.

Conventional SCM has two limitations: first, as it operates in contact mode, it can suffer from high imaging and shear forces, which links directly to tip lifetime, especially on structures with substantial topography variations. Second, it is operating at a fixed DC bias voltage between the tip and the sample, while lots of information becomes visible only when operating at a variety of voltages. In fact, cycling DC bias on every pixel has been a topic of interest for quite some time.[15] DCUBE-SCM overcomes these two limitations by providing high spatial and spectral resolution spectroscopic mapping data without the use of contact mode. By further analysis of the resulting data cubes, researchers can obtain additional information on oxide thickness, oxide charges, threshold voltages, contamination from mobile ions, and interface trap densities.

Figure 8 shows a DCUBE-SCM example from a SRAM transistor. In this measurement, the DC sample voltage was swept from -2 V to 2 V. The scan size was 2x2 μm^2 with 128x128 pixels. Each pixel took 100 ms and we collected the complete whole data cube in 27 min. Both the SCM dC/dV amplitude (displayed in Figure 8) and dC/dV phase data were also stored, in addition to the force-distance data. Visualization of the dC/dV amplitude data cube in a three-dimensional (3D) space of X, Y and VDC was created in MATLAB, shown in Figure 8a. The vertical plane shown in Figure 8b is a slice displaying the dynamic change of

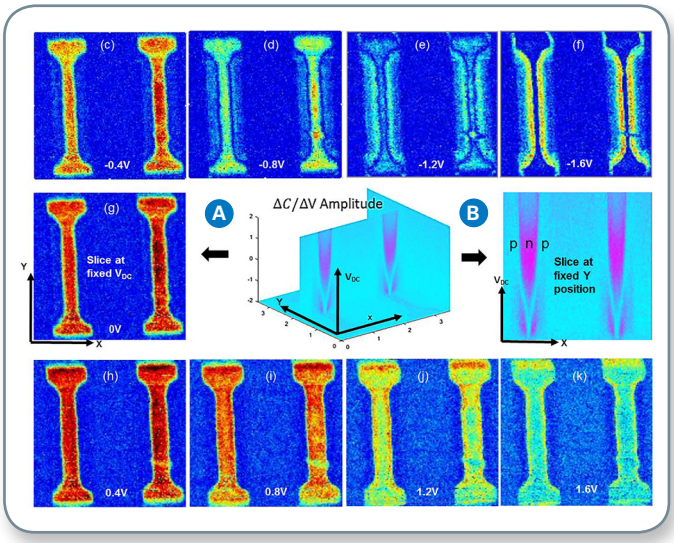

Figure 8. DCUBE-SCM study of two adjacent SRAM pnp transistors. This collection of images displays the SCM dC/dV amplitude data: (a) data cube in a 3D space of X, Y and VDC; (b) a slice of the data cube at a fixed Y position; (c)-(k) slices at selected, fixed DC biases along the VDC coordinate. DC sample voltage was swept from -2 V to +2 V. The scan size is 2x2 µm2 with 128x128 pixels.

dC/dV amplitude with VDC along the line in the X direction. This slice shows how the pnp junction carrier profile varies with the DC sample voltage and is a demonstration of the movement of "apparent junction," that is, effective channel length with DC voltage. Slices extracted at fixed DC voltages are shown in Figure 8c to 8k, where the fixed DC voltage is indicated on each image. Figure 8e and 8i show a defect on the right pnp junction. Interestingly, this defect is only visible at certain voltages, as shown in this series of data. This defect is better displayed by a movie of the whole collection of 128 slices.[18] This example illustrates that DataCube imaging allows one to observe effects easily missed when using conventional electrical modes operated at only a few discrete operating conditions.

Case Study: DataCube Scanning Microwave Impedance Microscopy (DCUBE–sMIM) on Delicate Samples

In sMIM, a microwave signal reflected from the tip-sample interface holds information of the electrodynamic properties of the sample surface underneath the tip apex.[8] Detecting and processing the reflectance in real time allows sMIM to directly access the permittivity and conductivity of the material. When an AFM-type sMIM probe is scanning across the sample surface, sMIM is capable of imaging variations in resistive (sMIM-R) and capacitive (sMIM-C) properties. This detection approach does not require making electrical contact between the sample and the substrate, as sMIM is based on the capacitive coupling between the tip and the sample. By AC-biasing the sample, sMIM also provides carrier profiling (dC/dV) capability similar

to traditional SCM. In the same way, it also uniquely offers mapping of nonlinear resistive properties (dR/dV). With both DC and AC sMIM signals, sMIM is suitable for studying surfaces with complex composition and over a broad dynamic range, e.g., metallic, semiconducting and insulating domains. As a near field method, the resolution of sMIM is limited by the tip radius of the probe and it can easily achieve a lateral resolution of <30 nm for electrical mapping. Sub-aF sensitivity and high signal/noise ratios are realized by using waveguide tips with coaxial shielding. When combined with PeakForce Tapping, it is possible to obtain sMIM results on delicate samples such as carbon nanotubes, and simultaneously acquire mechanical sample properties such as modulus and adhesion.[8] With DCUBE-sMIM one can acquire the same properties at a variety of sample voltages, in a single scan and get the "full picture" at once.

Doped Si Device

Figure 9 shows a DCUBE-sMIM example collected on a series of doped Si devices. The adhesion map is extracted directly from the force-distance spectra available in each pixel, and can, for example, be used to identify contamination. Both C-V and dC/dV-V spectra were collected in each pixel resulting in C, dC/dV amplitude, and dC/dV phase maps for voltages ranging from -2 V and +2 V. As an example, the dC/dV amplitude voltages at some discrete sample voltages are displayed, illustrating how the observed contrast strongly varies with applied voltage and carrier type and concentration.

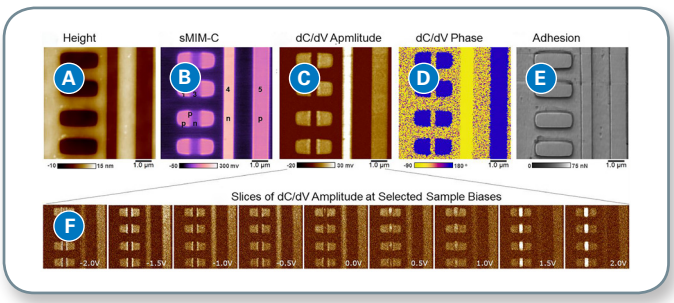

Figure 9. DCUBE- sMIM data acquired while ramping the sample bias from -2 V to +2 V. As an example, slices of the dC/dV amplitude data-cube at selected voltages are displayed and show voltage dependent contrast for some regions. Adhesion and Height are measured simultaneously and also displayed.

Si with Staircase Carrier Profile

Figure 10 shows typical data extracted from a DCUBE-sMIM study. In this example, we used a Si sample with a n-type and p-type staircase carrier profile, which forms a candidate sample for quantification of AFM-based carrier profiling methods.[32] Both the C-V spectra (sMIM-C vs sample bias) and R-V spectra (sMIM-R vs sample bias) were collected within 100 ms per pixel, covering a bias range of -2 V to +2 V. Having images over this bias range helps to differentiate and locate all carrier levels

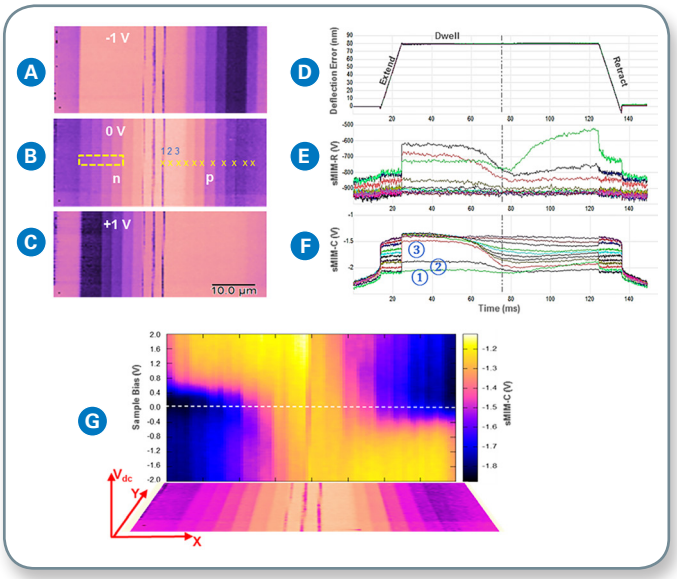

Figure 10. DCUBE-sMIM study of a Si sample with n-type and p-type staircase carrier profile: (a)–(c) 'sMIM-C' capacitance image slices at selected sample biases; (d)–(f) eleven spectral sets of force, sMIM-R and sMIM-C, respectively, collected at user-selected positions marked on (b); (g) slice image representing the sMIM-C signal vs sample bias and X position at a fixed Y location.

and regions in the sample. This is seen in the sMIM-C data in Figure 10a-c. The negative bias in Figure 10a drives the p-type regions into depletion regime, enhancing their contrast. The n-type regions are in the inversion regime, depressing their contrast, while the positive bias in Figure 10c has the opposite effect. Figure 10g combines this information in a single spatio-spectral slice.

DCUBE-sMIM provides valuable nanoelectrical information not only during the surface hold time, but also during the "approach" and "retract" processes. This is seen in Figure 10d-f, which are spectra taken at the locations marked by X in Figure 10b. First, during the hold time, the sMIM-C signals in Figure 10e show a gradual change in slope with carrier density. Most curves were taken in the p-type region. At negative bias, the sample is in the accumulation regime, causing equally high sMIM-C signal, which then drops as the bias turns positive and the sample goes into depletion. The signal drops further for lower doped regions. Second, Figure 10e and 10f also capture the sMIM signals before the probe touches and before bias is applied, thus automatically capturing the distance dependence.

Fitting of the sMIM-C versus distance spectra allows extraction of tip-shape information. One can easily extract the capacitance image at a given, fixed height above the sample. This image represents the "background" or stray capacitance, and can be subtracted from all capacitance data to remove background effects. This enhances the sMIM-C data, removes any stray capacitance effects, and provides a path for quantification of the sMIM-C data.

Detailed analysis and comparison of the sMIM signal during the "extend" and "retract" period also provides additional information. For example, asymmetric behaviors indicate a change of the sample surface after the dwell time.

Maghemite (γ-Fe_2O_3)

Figure 11 is an example of a DCUBE-sMIM study on a γ-Fe_2O_3 sample, where the electrical conditions were held constantly during the measurement and the sMIM signals were measured over time during the dwell period. Figure 11a shows γ-Fe_2O_3 spindle-like nanoparticles (100x500 nm in size) deposited into a continuous film. The corresponding adhesion map extracted from each force ramping cycle is shown in Figure 11b. This sample

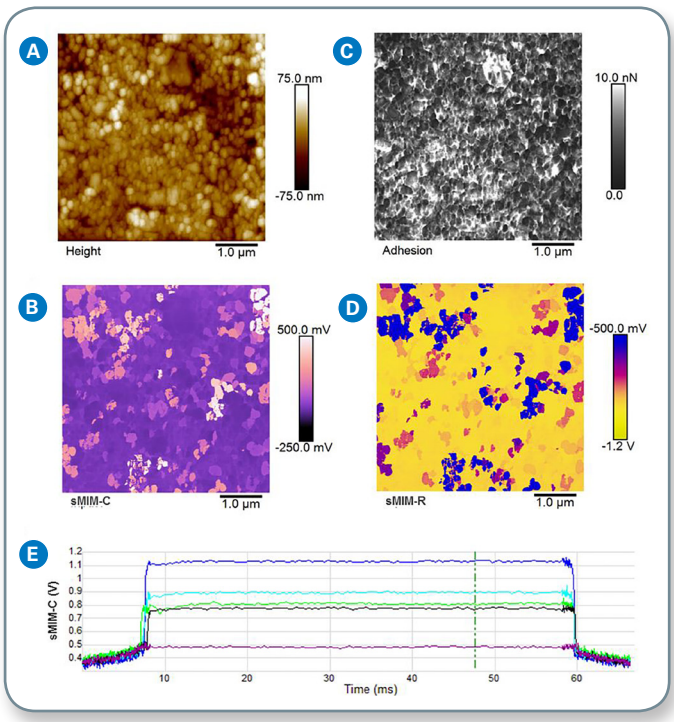

Figure 11. DCUBE-sMIM study of a γ-Fe_2O_3 sample: (a) surface topography; (b) quantitative adhesion map; (c) a slice of sMIM-C from the DCUBE results; (d) a slice of sMIM-R from the DCUBE results.

has conductivity inhomogeneity across the surface, and has been used as a reference sample in conductive AFM modes as already illustrated in Figures 3 and 4. The local impedance of the sample varies across the sample surface and shows contrast on both the sMIM-C and sMIM-R channels, as shown in Figures 11c and 11d. Figure 11e shows sMIM-C spectra at locations with different dielectric constants. As the probe approaches the surface, the sMIM-C signal shows the expected increase. Upon the snap-in contact at ~8 ms, the sMIM-C signal abruptly increases. Following this, as the force increases or tip indents into the sample for <1 ms, the tip-sample interaction interface area increases, resulting in further signal increase. During the dwell period, the sMIM signals are detected for 50 ms, while all electrical conditions are kept unchanged, allowing one to average over a relatively long period, achieving excellent signal/noise ratios in the sMIM maps.

Case Study: DataCube Piezoresponse (Piezoforce) Microscopy (DCUBE-PFM) on Piezoelectric Films

Piezoresponsive materials are substances that undergo mechanical deformation in response to an applied voltage. The properties of piezoresponsive materials make them useful in a wide range of areas, from microelectromechanical systems (MEMS) to biosensors. Ferroelectric materials are a subset of piezoelectrics that have particularly advantageous functional properties. As process control improves and fabrication of small volume ferroelectrics becomes more common, researchers have discovered that the physical characteristics of these materials change as they shrink. PFM enables high-resolution nanoscale characterization of piezoresponsive materials and topographical imaging. PFM is a contact AFM technique to measure sample displacement in response to an applied AC bias. The resulting cantilever deflection of the probe in contact with the sample is detected then demodulated by use of a lock-in amplifier, such that topography and ferroelectric domains can be imaged simultaneously with high resolution. PFM has also been widely used for domain writing and ferroelectric switching studies.[33-35] Integration with the data cube technique, DCUBE-PFM enables simultaneous acquisition of nanomechanical mapping and PFM amplitude/phase spectra in every pixel, revealing the switching behavior of each individual domain in a single data set. In addition, DCUBE-PFM overcomes artifacts, sample damage, and complexity of data analysis associated with the conventional contact mode based approach.

Figure 12 shows an example of DCUBE-PFM studies of a $BiFeO_3$ (BFO) piezoelectric film. In this experiment, the sample voltage is ramped from -6 V to 0 V during the dwell period while collecting the PFM amplitude and phase signals. Figure 12a shows the surface topography; a flat film with roughness of 0.37 nm. A PFM amplitude slice at -4.5 V

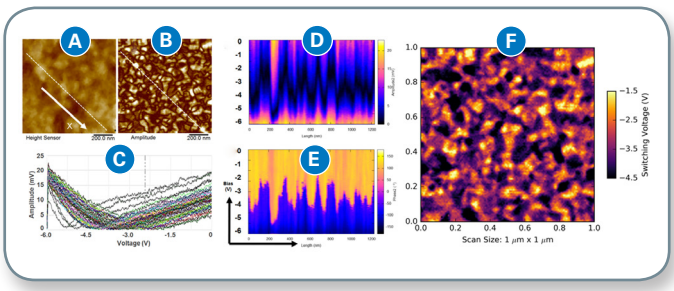

Figure 12. DCUBE-PFM studies of a BiF_eO_3 (BFO) piezoelectric film: (a) height; (b) PFM amplitude image; and (c) 50 of the selected 110 spectra along a 1.2 µm long line as indicated in (a) and (b), crossing multiple domains in a BFO ferro-electric sample; (d) and (e) plots of those 110 spectra show both PFM amplitude and PFM phase vs. bias during a ramp from -6 V to 0 V; (f) map of switching voltages extracted from the data cube.

differentiates different piezoelectric domains (Figure 12b). Figure 12c shows the first 50 of the selected 110 spectra along a 1.2 µm long line, as indicated by the white dashed lines in Figure 12a and 12b, crossing multiple domains in this BFO ferroelectric sample. These spectra indicate distinct switching voltages among different domains as the minimum of each spectrum spreads from about -5.0 V to -2.0 V on Figure 12c. These switching voltages can be extracted for each individual domain by the analysis of the spectra. Figure 12d and 12e are color plots of those 110 amplitude and phase spectra, respectively. The abrupt changes in color along the voltage (vertical) direction show the locations of the switching voltages. Further analysis of the data cube enables the extraction of the switching voltage at every pixel. These switching voltages can be plotted in a new map (Figure 12f) that shows that heterogeneous piezoelectric properties are present between domains and also within some single domains.

Figure 13 presents the same data cube results in a different format. Figure 13a and 13b respectively show two set of amplitude and phase spectra from two domains. Sample biases for the minimum of the amplitude spectra or the rise of the phase spectra indicate the switching voltages for the corresponding pixel on the XY plane. Figure 14c and 14d show the amplitude and phase data cubes, respectively.[19] The horizontal directions, X and Y, correspond to the scan area of the sample, which is 1x1 µm^2. The vertical direction, Z, from bottom to the top, is following the time of the hold segment while the sample bias was linearly applied from -6 V to 0 V. The size of this cube is 128x128x833 pixels. The four horizontal planes correspond to the slices of amplitude or phase at different sample biases. To better show the domain boundaries, the middle slice in the phase cube is shown as a set of contours over the range of values appearing at this bias. The two vertical slices along the XZ direction represent amplitude or phase changing over the

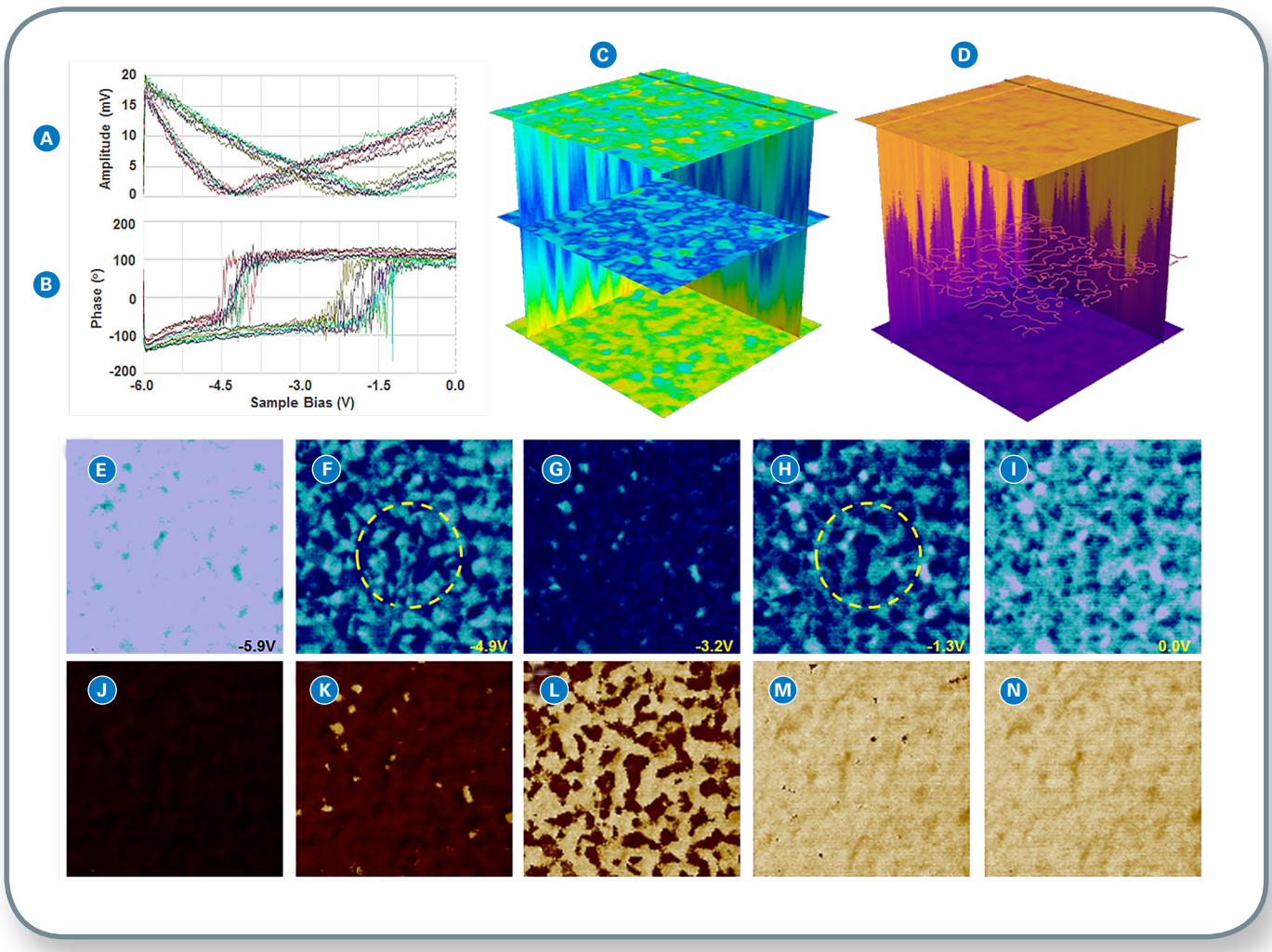

Figure 13. DCUBE-PFM studies of a $BiFeO_3$ (BFO) piezoelectric film: (a) two sets of amplitude spectra from two different domains inside the red circles in (f) and (h); (b) corresponding phase spectra to those in (a); (c) and (d) are cubes of the amplitude and phase data, respectively. X and Y correspond to the 1 µm x 1 µm scan area. The vertical direction, Z, from bottom to the top, is the sample bias from -6 V to 0 V. The cube color represents the amplitude or phase in the cube space, i.e., the measured PFM signal at a specific XY location and applied bias. The cube size is 128x128x833 (or 1x1 µm2 x 6 V). The four horizontal planes correspond to the slices of amplitude or phase at different sample bias. The middle slice in the phase cube is shown as a set of contours over the range of values appearing at this bias. The two vertical slices along the XZ direction represent amplitude or phase changing over the sample bias (Z direction) along two line positions in the XY plane. (e)-(i) are slices of amplitude at different sample bias; and (j)-(n) are slices of phase at different sample bias.

sample bias (Z direction) along two line positions in the XY plane. Figure 13e-13i are slices of amplitude at different sample bias, extracted from data cube.

Case Study: DCUBE – Contact Resonance (CR) PFM on a $LiTAO_3$ Sample

In PFM, the applied AC bias of a certain frequency results in a periodic AC deformation of the sample surface at the same frequency. Operation at or near the contact resonance has been exploited in PFM to provide enhanced piezoelectric response signal.[36,37] For a single-frequency PFM measurement, the implementation of this technique is limited, as the contact resonance shifts with the nature of the tip-sample contact as well as with the sample material properties. DCUBE-CR PFM overcomes this challenge, where during the dwell duration the frequency is swept to collect a complete contact resonance spectrum. This hybrid mode inherits all advantages from the FASTForce Volume Contact Resonance mode (FFV-CR) developed for characterization of viscoelastic mechanical properties[5]:

- frequency sweeps can be performed over a broad range (up to 5 MHz) enabling observation and tracking of multiple eigenmodes at once;
- resonance frequency and quality factor can be extracted with a real-time fit of the spectrum, and can be calculated into loss modulus, storage modulus, and loss tangent when applying the proper mechanical model;
- adhesion, stiffness and modulus are extracted out of the force-distance spectrum; and
- piezoelectric properties can be extracted out of the phase and amplitude signals, in particular at the resonance frequency.

Figure 14a to 14c shows some typical DCUBE-CR PFM force ramping, PFM phase, and PFM amplitude spectra of a $LiTaO_3$ (LTO) sample. In this measurement, the frequency was ramped from 250 to 400 kHz in every pixel during a 100 ms dwell period. Figure 15d and 15e shows the phase and amplitude data cubes, respectively.[19] The size and the space pixel density of these two cubes are 3x3 μm^2 x 150 kHz and 256x256x260. The horizontal planes show phase (Figure 14d) or amplitude (Figure 14e) maps at specific frequencies, where different piezoelectric domains are well differentiated at and near contact resonance. Vertical planes are phase (Figure 14d) or amplitude (Figure 14e) changing with the sweep frequency, which

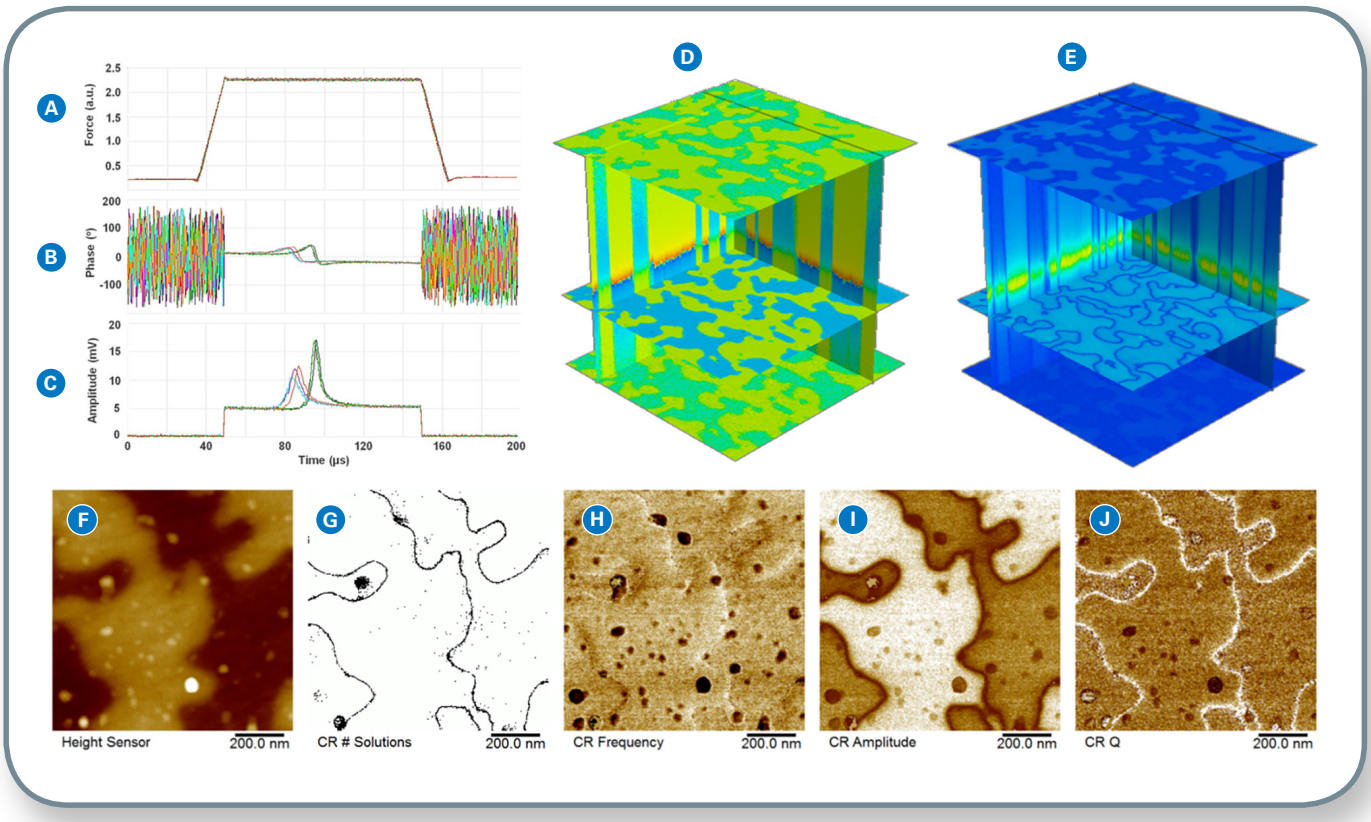

Figure 14. DCUBE-CR PFM studies on a $LiTaO_3$ sample: (a)-(c) typical DCUBE-CR PFM force ramping, PFM phase, and PFM amplitude spectra, respectively, frequency swept from 250 to 400 kHz during the 100 ms dwell period; (d)-(e) visualization of the phase and amplitude data cubes, respectively, where XY are the scan area and z is the frequency sweep. Size is 3x3 μm^2 x 150 kHz, and the pixel density is 256x256x260. Horizontal planes show phase or amplitude maps at specific frequencies. Vertical planes are phase or amplitude changing over the sweep frequency. (f) Surface topography, at scan 1x1 μm^2 scan size; (g) number of valid solutions found for the characteristic equation from which stiffness and damping are determined; (h)-(i) maps of contract resonance frequency, amplitude, and quality factor found upon fitting the hold sweep spectra.

demonstrates shifts in the contact resonance frequency between different domains. Figure 14f-14j shows the DCUBE-CR PFM data on the same $LiTaO_3$ sample with a smaller scan size of 1x1 μm^2. Figure 14f is the surface topography with a roughness (Rq) of ~1.5 nm. Figure 14g shows the number of peak that the algorithm found during the fitting. At the domain boundaries and in some contaminant positions, this signal becomes zero indicating that the material does not show piezoelectric response. The "CR Frequency," "CR Amplitude," and "CR Q" channels in (h)-(i) are maps of contact resonance frequency, amplitude, and quality factor found upon fitting the hold sweep spectra. This example demonstrates that DCUBE-PFM in conjunction with contact resonance provides the full benefits of DCUBE-PFM with the added benefits of providing a frequency ramp at every pixel, providing a full spectrum and the peak sensitivity at the contact resonance.

Conclusions

DCUBE-based nanoelectrical modes represent a general big data approach with the potential to provide new information in a wide range of applications, especially on samples with high complexity. Extracting image slices, spatio-spectral slices, or spectra at every pixel opens the door to reveal sample properties that are either not accessible or are easily missed in conventional nanoelectrical modes, where images at only one or a few discrete settings are acquired. Table 2 shows the favorable comparison of DCUBE modes to contact and PeakForce Tapping modes.

	Contact Mode	PeakForce Tapping	DataCube
Samples	Challenging on soft and fragile sample	All samples	All samples
Correlation to Mechanical properties	No	Integrated	Integrated
High dimensional electrical data (= at different electrical settings)	No	No	Yes
Maps of new electrical properties (flat-band voltage, barrier height, switching voltage,...)	No	No	Yes
Speed per image	Standard afm imaging speed	Standard afm imaging speed	Slightly slower
Tip lifetime	Limited on certain samples	Excellent	Excellent

Table 2. DCUBE-based electrical modes are compared to contact mode and PeakForce Tapping–based electrical modes.

The DataCube approach is also applicable to many AFM-based electrical characterization modes, including TUNA, SCM, SSRM, sMIM and PFM, allowing researchers to study spectral data over a variety of operating conditions. Other advantages include: large data content with full spectral information and images at a range of operating conditions, embedded in a single data set; correlation between electrical and mechanical properties; elimination of contact mode, resulting in longer tip lifetime, and the capability to measure soft and fragile samples; and mapping of new nanoelectrical properties, such as schottky barrier height, flatband voltages, piezoelectric switching voltages, etc. Finally, each individual nanoelectrical mode is improved with the DataCube approach, including, for example, the capability to measure and subtract background capacitance contributions in sMIM and PFM data acquisition at the highest sensitivity using a contact resonance approach.

Authors

P. De Wolf[a], Z. Huang[b], B. Pittenger[c], A. Dujardin[a,b], M. Febvre[a], D. Mariolle[c], N. Chevalier[c]

a. Bruker Nano Surfaces, 112 Robin Hill Road, Santa Barbara, CA 93117, USA

b. Cellular Microbiology and Physics of Infection Group – Lille Centre for Infection and Immunity, CNRS UMR8204, INSERM U1019, Lille Regional Hospital University Centre, University of Lille, Institut Pasteur de Lille, F-59021 Lille, France

c. Univ. Grenoble Alpes, CEA, LETI, 3800 Grenoble, France

References

1. Pittenger, B., Erina, N. and Su, C., "Quantitative Mechanical Property Mapping at the Nanoscale with PeakForce QNM," *Bruker Application Note* 128 (2012).

2. Pittenger, B. and Yablon, D. G., "Improving the Accuracy of Nanomechanical Measurements with Force-Curve-Based AFM Techniques," *Bruker Application Note* 149 (2017).

3. Berquand, A., "Quantitative Imaging of Living Biological Samples by PeakForce QNM Atomic Force Microscopy," *Bruker Application Note* 135 (2011).

4. Kaemmer, S. B., "Introduction to Bruker's ScanAsyst and PeakForce Tapping AFM Technology," *Bruker Application Note* 133 (2011).

5. Pittenger, B. and Yablon, D. G., "Quantitative Measurements of Elastic and Viscoelastic Properties with FASTForce Volume CR," *Bruker Application Note* 148 (2017).

6. Li, C., Minne, S., Pittenger, B. and Mednick, A., "Simultaneous Electrical and Mechanical Property Mapping at the Nanoscale with PeakForce TUNA." *Bruker Application Note* 132 (2011).

7. Li, C. et al., "PeakForce Kelvin Probe Force Microscopy," *Bruker Application Note* 140 (2013).

8. Huang, Z. et al., "Nanoscale Mapping of Permittivity and Conductivity with Scanning Microwave Impedance Microscopy," *Bruker Application Note* 145 (2016).

9. Calahorra, Y., Smith, M., Datta, A., Benisty, H. and Kar-Narayan, S., "Mapping Piezoelectric Response in Nanomaterials Using a Dedicated Non-Destructive Scanning Probe Technique," *Nanoscale* 9, 19290-97 (2017).

10. Huang, Z. et al., "An Introduction to AFM-Based Scanning Electrochemical Microscopy: PeakForce SECM," *Bruker Application Note* 147 (2017).

11. Jiang, J. J. et al., "Nanoelectrical and Nanoelectrochemical Imaging of Pt/p-Si and Pt/p+-Si Electrodes," *Chemsuschem* 10, 4657-63 (2017).

12. Nellist, M. R. et al., "Atomic Force Microscopy with Nanoelectrode Tips for High Resolution Electrochemical, Nanoadhesion and Nanoelectrical Imaging," *Nanotechnology* 28, 095711 (2017).

13. Nellist, M. R. et al., "Potential-Sensing Electrochemical Atomic Force Microscopy for in operando Analysis of Water-Splitting Catalysts and Interfaces. *Nat Energy* 3, 46-52 (2018).

14. Toma, F. M., "Disentangling Interfacial Energetics," *Nat Energy* 3, 6-7 (2018).

15. Edwards, H. et al., "Scanning Capacitance Spectroscopy: An Analytical Technique for pn-Junction Delineation in Si Devices," *Appl Phys Lett* 72, 698-700 (1998).

16. Yang, S. M. et al., "Humidity Effect on Nanoscale Electrochemistry in Solid Silver Ion Conductors and the Dual Nature of Its Locality," *Nano Lett* 15, 1062-69 (2015).

17. De Wolf, P. et al., "Data Cube Modes: Enabling Functional Imaging with Higher Dimensional Electrical Data Sets," *Microscopy Today* (2018).

18. Bruker NanoElectrical Lab, https://www.bruker.com/products/surface-and-dimensional-analysis/atomic-force-microscopes/nanoelectrical-lab.html (2019).

19. Ramachandran, P. and Varoquaux, G., "Mayavi: 3D Visualization of Scientific Data," *Comput Sci Eng* 13, 40-50 (2011).

20. Palacin, M. R. and de Guibert, A., "Why Do Batteries Fail?" *Science* 351, 1253292 (2016).

21. Semenov, A. E., Borodina, I. N. and Garofalini, S. H., "In Situ Deposition and Ultrahigh Vacuum STM/AFM Study of V2O5/Li3PO4 Interface in a Rechargeable Lithium-Ion Battery," *J Electrochem Soc* 148, A1239-46 (2001).

22. Becker, C. R., Prokes, S. M. and Love, C. T., "Enhanced Lithiation Cycle Stability of ALD-Coated Confined a-Si Microstructures Determined Using In Situ AFM," *Acs Appl Mater Inter* 8, 530-37 (2016).

23. Hernandez, G. et al., "Redox-Active Polyimide-Polyether Block Copolymers as Electrode Materials for Lithium Batteries," *Rsc Adv* 5, 17096-103 (2015).

24. Hiesgen, R. et al., "AFM As an Analysis Tool for High-Capacity Sulfur Cathodes for Li-S Batteries," *Beilstein J Nanotech* 4, 611-24 (2013).

25. Chen, J. C., Yan, Y. D., Sun, T., Qi, Y. and Li, X. D., "Deformation and Fracture Behaviors of Microporous Polymer Separators for Lithium Ion Batteries," *Rsc Adv* 4, 14904-14 (2014).

26. Breitung, B., Baumann, P., Sommer, H., Janek, J. and Brezesinski, T., "In Situ and Operando Atomic Force Microscopy of High-Capacity Nano-Silicon Based Electrodes for Lithium-Ion Batteries," *Nanoscale* 8, 14048- 56 (2016).

27. Shen, C. et al., "Direct Observation of the Growth of Lithium Dendrites on Graphite Anodes by Operando EC-AFM," *Small Methods* 2, 1700289 (2018).

28. Wang, S. W. et al., "Operando Study of Fe3O4 Anodes by Electrochemical Atomic Force Microscopy," *Appl Surf Sci* 426, 217-23 (2017).

29. Kumar, R. et al., "In Situ and Operando Investigations of Failure Mechanisms of the Solid Electrolyte Interphase on Silicon Electrodes," *Acs Energy Lett* 1, 689-97 (2016).

30. Wang, S. W., Yang, K., Gao, F., Wang, D. Y. and Shen, C., "Direct Visualization of Solid Electrolyte Interphase on Li4Ti5O12 by In Situ AFM," *Rsc Adv* 6, 77105-10 (2016).

31. Kitta, M. and Kohyama, M., "Stability of the LiMn2O4 Surface in a LiPF6-Based Non-Aqueous Electrolyte Studied by In-Situ Atomic Force Microscopy," *Jpn J Appl Phys* 55 (2016).

32. Schweinbock, T. and Hommel, S., "Quantitative Scanning Microwave Microscopy: A Calibration Flow," *Microelectron Reliab* 54, 2070-74 (2014).

33. Gruverman, A., Auciello, O. and Tokumoto, H., "Imaging and Control of Domain Structures in Ferroelectric Thin Films Via Scanning Force Microscopy," *Annu Rev Mater Sci* 28, 101-23 (1998).

34. Wang, C. S. et al., "Ferroelastic Switching in a Layered-Perovskite Thin Film," *Nat Commun* 7, 10636 (2016).

35. C., A. J. et al., "Machine Detection of Enhanced Electromechanical Energy Conversion in PbZr0.2Ti0.8O3 Thin Films," *Advanced Materials* 30, 1800701 (2018).

36. Harnagea, C., Alexe, M., Hesse, D. and Pignolet, A., "Contact Resonances in Voltage-Modulated Force Microscopy," *Appl Phys Lett* 83, 338-40 (2003).

37. Harnagea, C., Pignolet, A., Alexe, M. and Hesse, D., "Higher-Order Electromechanical Response of Thin Films by Contact Resonance Piezoresponse Force Microscopy," *IEEE T Ultrason Ferr* 53, 2309-22 (2006).

©2019 Bruker Corporation. FASTForce Volume, NanoScope, PeakForce QNM, PeakForce Tapping, and PeakForce TUNA are trademarks of Bruker Corporation. All other trademarks are the property of their respective companies. All rights reserved. AN152, Rev. A0.

Bruker Nano Surfaces Division
Santa Barbara, CA · USA
phone +1.805.767.1400
productinfo@bruker.com
www.bruker.com/nano